BRAF inhibitor resistance mediated by the AKT pathway in an oncogenic BRAF mouse melanoma model

Daniele Perna[a,b,1,2], Florian A. Karreth[b,1,3], Alistair G. Rust[a], Pedro A. Perez-Mancera[b], Mamunur Rashid[a], Francesco Iorio[c,d], Constantine Alifrangis[c], Mark J. Arends[e], Marcus W. Bosenberg[f], Gideon Bollag[g], David A. Tuveson[b,h,4], and David J. Adams[a,4]

[a]Experimental Cancer Genetics and [c]Cancer Genome Project, Wellcome Trust Sanger Institute, Hinxton, Cambridge CB10 1SA, United Kingdom; [b]Cancer Research UK Cambridge Institute, University of Cambridge, Cambridge CB2 0RE, United Kingdom; [d]European Molecular Biology Laboratory, European Bioinformatics Institute, Hinxton, Cambridge CB10 1SA, United Kingdom; [e]University of Edinburgh Division of Pathology, Edinburgh Cancer Research Centre, Institute of Genetics & Molecular Medicine, Western General Hospital, Edinburgh, EH4 2XR, United Kingdom; [f]Department of Dermatology, Yale University, New Haven, CT 06520; [g]Plexxikon Inc., Berkeley, CA 94710; and [h]Cold Spring Harbor Laboratory, Cold Spring Harbor, NY 11724

Edited by Neal G. Copeland, Houston Methodist Research Institute, Houston, TX, and approved December 30, 2014 (received for review September 20, 2014)

BRAF (v-raf murine sarcoma viral oncogene homolog B) inhibitors elicit a transient anti-tumor response in ∼80% of *BRAF*^{V600}-mutant melanoma patients that almost uniformly precedes the emergence of resistance. Here we used a mouse model of melanoma in which melanocyte-specific expression of *Braf*^{V618E} (analogous to the human *BRAF*^{V600E} mutation) led to the development of skin hyperpigmentation and nevi, as well as melanoma formation with incomplete penetrance. *Sleeping Beauty* insertional mutagenesis in this model led to accelerated and fully penetrant melanomagenesis and synchronous tumor formation. Treatment of *Braf*^{V618E} transposon mice with the BRAF inhibitor PLX4720 resulted in tumor regression followed by relapse. Analysis of transposon insertions identified eight genes including *Braf, Mitf*, and *ERas* (ES-cell expressed Ras) as candidate resistance genes. Expression of *ERAS* in human melanoma cell lines conferred resistance to PLX4720 and induced hyperphosphorylation of AKT (v-akt murine thymoma viral oncogene homolog 1), a phenotype reverted by combinatorial treatment with PLX4720 and the AKT inhibitor MK2206. We show that *ERAS* expression elicits a prosurvival signal associated with phosphorylation/inactivation of BAD, and that the resistance of hepatocyte growth factor-treated human melanoma cells to PLX4720 can be reverted by treatment with the BAD-like BH3 mimetic ABT-737. Thus, we define a role for the AKT/BAD pathway in resistance to BRAF inhibition and illustrate an in vivo approach for finding drug resistance genes.

melanoma | drug resistance | BRAF inhibitors | mouse models

The discovery that ∼50–60% of melanomas carry *BRAF*^{V600E} point mutations (1) prompted the generation of compounds specifically targeting this hyperactive mutated kinase. One such compound, PLX4032, has shown unprecedented therapeutic efficacy in clinical trials and was therefore FDA-approved for clinical therapy under the name vemurafenib. Despite its remarkable efficacy, almost all patients receiving BRAF inhibitor treatment relapsed after weeks to months of therapy (2–5). Acquired resistance to BRAF inhibitors has since been a major focus of research and two major paths to resistance have emerged: MAPK-dependent and MAPK-independent mechanisms. MAPK-dependent mechanisms primarily involve reactivation of the MAPK pathway to substitute for the inhibition of BRAF^{V600E}. This may be achieved through mechanisms including expression of alternative splicing forms of *BRAF*^{V600E}, amplification of *BRAF*^{V600E}, the acquisition of activating mutations in *NRAS* or *MEK* (*MAP2K1*), or loss of *NF1*. Similarly, *COT* (*MAP3K8*) overexpression has been shown to drive resistance through ERK activation independent of RAF signaling (6–11). Elevated signaling through the PI3K/AKT pathway, with or without concomitant MAPK reactivation, represents an alternative path to resistance. Indeed, AKT signaling mediated by several genetic lesions including increased expression of the *insulin-like growth factor 1 receptor* (*IGF1R*) and expression of hepatocyte growth factor (*HGF*) by stromal cells has been linked to BRAF inhibitor resistance (12–14). Similarly, activation of the PI3K pathway through loss of *PTEN,* or deregulation of other genes (e.g., *AKT3*, *BCL2A1*, *IGF1*, and *PIB5PA*), has been shown to result in resistance to BRAF inhibitor-induced apoptosis (15–19). Additional mediators of resistance have also been proposed, including upregulation of the tyrosine kinase *platelet-derived growth factor receptor beta* (*PDGFRB*), possibly through MAPK- or PI3K-related mechanisms (8).

We generated a mouse model of *Braf*^{V618E}-induced melanoma (analogous to *BRAF*^{V600E} in humans; transcript ENSMUSE00000277767 in mouse) and used it in combination

Significance

Using *Sleeping Beauty* transposon mutagenesis in a melanoma model driven by oncogenic BRAF (B-Raf proto-oncogene, serine/threonine kinase), we identified both known and novel candidate genes that mediate resistance to the BRAF inhibitor PLX4720. We validate ES-cell expressed Ras as a novel promoter of BRAF inhibitor resistance and propose that AKT (v-akt murine thymoma viral oncogene homolog 1)-mediated inactivation of BAD (BCL2-associated agonist of cell death) constitutes a pathway that may contribute to hepatocyte growth factor-mediated therapy resistance. Our work establishes *Sleeping Beauty* mutagenesis as a powerful tool for the identification of novel resistance genes and mechanisms in genetically modified mouse models.

Author contributions: D.P., F.A.K., D.A.T., and D.J.A. designed research; D.P., F.A.K., F.I., and C.A. performed research; P.A.P.-M., M.W.B., and G.B. contributed new reagents/analytic tools; D.P., F.A.K., A.G.R., M.R., F.I., and M.J.A. analyzed data; and D.P., F.A.K., D.A.T., and D.J.A. wrote the paper.

Conflict of interest statement: G.B. is an employee of Plexxikon Inc., which owns and markets vemurafenib.

This article is a PNAS Direct Submission.

Freely available online through the PNAS open access option.

Data deposition: The sequence reported in this paper has been deposited in the European Nucleotide Archive (accession no. ERP002600).

[1]D.P. and F.A.K. contributed equally to this work.

[2]Present address: Biopharm Discovery Process, GlaxoSmithKline, Stevenage SG1 2NY, United Kingdom.

[3]Present address: Meyer Cancer Center, Weill Cornell Medical College, New York, NY 10021.

[4]To whom correspondence may be addressed. Email: dtuveson@cshl.edu or da1@sanger.ac.uk.

This article contains supporting information online at www.pnas.org/lookup/suppl/doi:10.1073/pnas.1418163112/-/DCSupplemental.

with *Sleeping Beauty* insertional mutagenesis to identify mechanisms of resistance to BRAF inhibition using PLX4720, a vemurafenib analog. As in patients with tumors carrying $BRAF^{V600}$ mutations, melanomas in our mouse model showed an initial response to BRAF inhibitor treatment, characterized by rapid tumor regression, followed by tumor recurrence after weeks to months of therapy. Analysis of transposon insertion sites in naïve and PLX4720-resistant melanomas identified the proto-oncogene *ERas,* and seven other genes, as putative mediators of resistance. We show that *ERAS* expression confers resistance associated with inactivation of the proapoptotic protein BAD in an AKT/PI3K-dependent manner, and that BAD also contributes to BRAF inhibitor resistance in the context of activated HGF signaling. These data illustrate the human relevance of genes/pathways found through insertional mutagenesis screens for drug resistance mediators.

Results

Targeted Expression of Oncogenic $Braf^{V618E}$ Induces Skin Hyperpigmentation, Nevi, and Melanoma. We targeted the endogenous murine *Braf* locus by introducing a stop element (*LoxP-Stop-LoxP* or *LSL* cassette) into intron 2 and a *V618E* mutation into exon 15 (Fig. 1*A*). Our model is similar to other models (20, 21) with the exception of *FRT* sites in introns 2 and 14 to allow Flp-mediated conditional deletion of the mutant *Braf* allele (*SI Materials and Methods* and Fig. S1). Validation of the allele is shown in the *SI Materials and Methods*.

To target expression of the *Braf* oncogene specifically to melanocytes we intercrossed *LSL-*$Braf^{V618E}$ mice with the melanocyte-specific, 4-hydroxytamoxifen (4-OHT)-inducible *Tyrosinase-*$CreER^{T2}$ allele ($TyrCreER^{T2}$) (Fig. 1*A*) (22). Experiments were performed in *LSL-*$Braf^{V618E}$; $TyrCreER^{T2}$ heterozygotes owing to perinatal lethality of *LSL-*$Braf^{V618E}$ homozygotes (23).

To assess the biological effect of $Braf^{V618E}$ activation on the melanocyte compartment, 3- to 4-wk-old *LSL-*$Braf^{V618E/+}$*; Tyr-*$CreER^{T2}$ mice (hereby designated as BC mice) were shaved and their back skin, flanks, ears, and tail were treated topically with a 25 mg/mL solution of 4-OHT for two consecutive days. After ∼6–8 wk hyperpigmentation of treated areas and to a lesser extent all skin surfaces including the urogenital area and paws was observed, the latter being due to systemic spread of 4-OHT (Fig. S2*A*). Histological analysis of back and ear skin revealed a vast expansion of terminally differentiated, heavily pigmented melanocytes in BC mice treated with 4-OHT, but not in 4-OHT–treated controls ($Braf^{wt}$*;* $TyrCreER^{T2}$ mice) (Fig. S2 *A* and *C*).

One to two months after treatment numerous heavily pigmented nevi, primarily located on the trunk skin, were observed in 4-OHT–treated BC mice (Fig. S2*B*). Smaller melanocytic nevi showed melanin-producing cells that were primarily located in the dermis; some were scattered in the s.c. fat (Fig. S2*C*). Larger nevi showed collections of melanin-producing cells in the dermis, with these collections extending into the fat below (Fig. S2*D*). Furthermore, epithelioid blue nevi were infrequently observed, as previously reported (Fig. S2*E*) (21). These results are in keeping with the presence of *BRAF* mutations in up to 85% of melanocytic nevi in humans (24, 25).

Progression of melanocytic nevi to malignant melanoma is rare in humans, yet around 30–50% of melanomas develop from these benign tumors. Thus, we aged 4-OHT–treated BC mice to assess the penetrance of spontaneous tumor formation in our model. We observed that 87% of BC mice developed melanoma, primarily on the trunk and to a lesser extent on the extremities (Fig. S2*F*), similar to previous reports in analogous models (20, 21). The median latency of tumor formation was 426 d (Fig. 1*B*, green line) and the average multiplicity of tumor formation was 1. Given that each mouse was covered with hundreds to thousands of nevi, akin to atypical mole syndrome in humans, the transformation of melanocytic nevi to melanoma is exceedingly rare and suggests a requirement for additional genetic alterations for melanomagenesis. Those melanomas that did form were generally hypopigmented and primarily dermal (Fig. S2*G*). There was little or no epidermal involvement, and most tumors had a spindle-cell morphology. Tumors with predominant epithelioid cell features were rarely observed. Melanoma cells displayed characteristic enlarged and pleomorphic nuclei, sometimes with prominent eosinophilic atypical nucleoli and numerous mitotic figures (Fig. S2*H*). Larger lesions showed superficial ulceration, but with no or very little evidence of an intraepidermal invasive component (radial/horizontal growth phase) (Fig. S2*I*). Infiltration of melanoma cells through the underlying skeletal muscle and into s.c. adipose tissue was commonly observed (Fig. S2*J*). Occasionally melanomas showed foci of lymphocyte aggregates and scattered tumor-infiltrating lymphocytes (Fig. S2*K*). Residual pigmented melanocytes were observed in a subset of melanomas (Fig. S2*L*). Despite their predominantly amelanotic nature, tumors expressed the melanocyte lineage markers S100A and MITF (Fig. S2 *M* and *N*). At necropsy draining lymph nodes appeared brown in color and histological analysis revealed the presence of lightly pigmented as well as unpigmented melanoma cells with pleomorphic nuclei and also melanophages, which were heavily pigmented owing to phagocytosis of melanin (Fig. S2 *O* and *P*). Thus, oncogenic $Braf^{V618E}$ alone is sufficient to initiate melanomagenesis but with incomplete penetrance and with an extended latency, suggesting a requirement for additional genetic events.

***Sleeping Beauty* Insertional Mutagenesis Identifies Drivers of Melanoma Formation and Mediators of Resistance to the BRAF Inhibitor PLX4720.** To identify novel genes and pathways contributing to melanoma formation and to BRAF inhibitor resistance we performed a forward genetic screen using the *Sleeping Beauty* (SB) transposon system (26–28). BC mice were crossed with animals carrying elements of the SB transposon system to generate quadruple mutant BCTSB13 animals (*LSL-*$Braf^{V618E/+}$; *Tyrosinase-*$CreER^{T2}$; *T2/Onc*; *Rosa26-LSL-SB13*; Fig.1*A*) and triple mutant BCT littermate controls (*LSL-*$Braf^{V618E/+}$; *Tyrosinase-*$CreER^{T2}$; *T2/Onc*). Application of 4-OHT to the skin of BCTSB13 mice simultaneously induced expression of the $Braf^{V618E}$ mutant allele and transposon mobilization, with consequent induction of additional random somatic mutations (Fig. 1*A*). Insertional mutagenesis in BCTSB13 mice led to a dramatic acceleration of melanoma formation and a decrease in the median survival to ∼130 d ($P < 0.0001$) compared with BC or BCT mice, whose median survival was comparable (426 and 408.5 d, respectively) (Fig. 1*B*). Importantly, transposon activation in melanocytes not only accelerated tumorigenesis but also increased tumor multiplicity to an average of 3.6 tumors per mouse, with a few mice developing more than 10 synchronous melanomas (Fig. 1*C*). From a cohort of 78 BCTSB13 mice we collected 278 tumors for transposon insertion site analysis.

In parallel with the abovementioned study we randomly enrolled a cohort of 4-OHT–treated BCTSB13 mice for treatment with the BRAF inhibitor PLX4720 (29). Mice with melanomas of at least 200 mm^3 in size were transferred onto a standard laboratory diet containing PLX4720. An acute response to PLX4720 treatment was evident; melanomas initially regressed during the first 1–4 wk of treatment (Fig. 1*D*). Stable disease was maintained in BCTSB13 mice for an average of 76 d (Fig. 1 *D* and *E*) until relapse at the site of the initial tumor formation was observed. After relapse tumors were collected before reaching 10% of body weight. We harvested 53 PLX4720-resistant tumors from 30 mice from which we isolated genomic DNA for insertion site analysis. Importantly, comparison of PLX4720 levels by mass spectrometry of plasma, tissues (liver, spleen, skin, and salivary gland), and tumor material in mice carrying tumors either resistant or sensitive to PLX4720 revealed comparable concentrations of PLX4720 ranging from 200 μM in plasma to 70 μM in

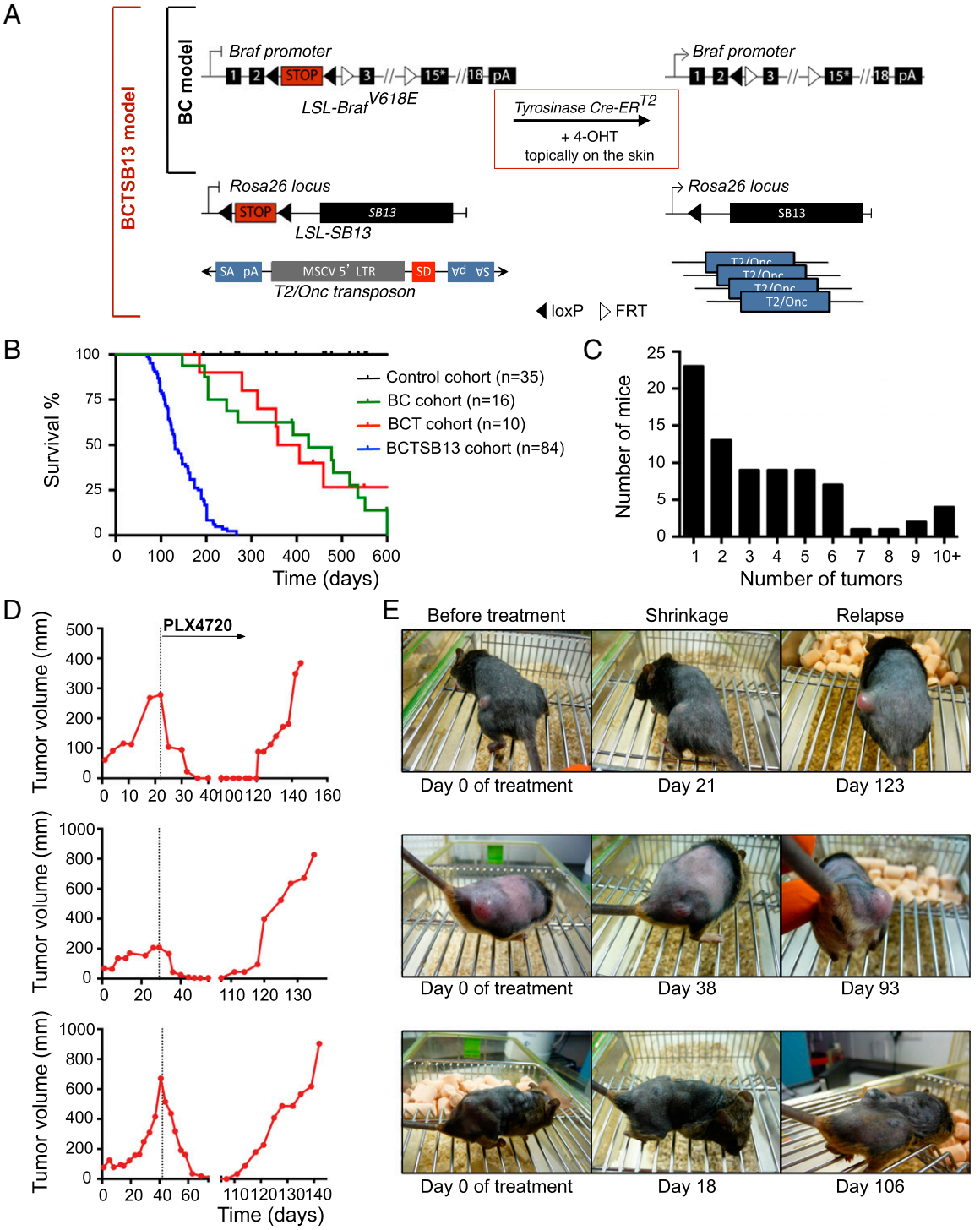

Fig. 1. *Sleeping Beauty* insertional mutagenesis accelerates $Braf^{V618E}$-induced melanoma development and induces resistance to PLX4720. (*A*) Scheme of the alleles in the *LSL-*$Braf^{V618E/+}$*; Tyrosinase-*$CreER^{T2}$ (or BC) and *LSL-*$Braf^{V618E/+}$*; Tyrosinase-*$CreER^{T2}$*; T2/Onc*; *Rosa26-LSL-SB13* (or BCTSB13) mouse models. Application of 4-OHT onto the skin of these mice activates $CreER^{T2}$ selectively in melanocytes, inducing the simultaneous expression of both oncogenic $Braf^{V618E}$ and *SB13* transposase. The *T2/Onc* transposon contains elements to elicit transcriptional activation such as the MSCV 5′ LTR and splice donor (SD), or inactivation such as splice acceptors (SA) and polyadenylation signals (pA). The position of LoxP sites (black arrowheads) and FRT sites (white arrowheads) are indicated. (*B*) Kaplan–Meier survival curve of 4-OHT–treated mice showing that BCTSB13 mice ($n = 84$) have a reduced median survival compared with BC mice ($n = 16$; median survival 131 vs. 426 d, $P < 0.0001$), BCT mice ($n = 10$; median survival 131 vs. 382 d, $P < 0.0001$), and control mice (BTSB13 and CTSB13 mice; $n = 35$; median survival >600 d, $P < 0.0001$). (*C*) Number of tumors developed in the cohort of 4-OHT–treated BCTSB13 mice; 70% of the mice developed more than one tumor. (*D*) Melanomas of 4-OHT–treated BCTSB13 mice first respond to PLX4720 and shrink but then relapse upon continuous, prolonged treatment. After appearance, tumor sizes were measured twice a week before and after the beginning of treatment with a PLX4720-containing diet (represented by the dotted line). Tumor volumes were calculated as described in *Materials and Methods*. Each mouse was placed on drug treatment once it had developed at least one melanoma of 200 mm^3. Mice were then continuously fed with the drug-containing diet until the endpoint. (*E*) Photographs showing BCTSB13 mouse melanomas before treatment (*Left*), at completed shrinkage (*Center*) and upon relapse (*Right*). The indicated days represent the duration of drug treatment.

the tumors and 6–30 μM in the other tissues (Fig. S3). This suggests that drug efflux does not contribute significantly to PLX4720 resistance in our model.

Furthermore, to rule out the possibility that drug resistance is due to mechanisms not mediated by transposon insertion events we performed whole-exome sequencing of six BCTSB13-resistant tumors, revealing no acquired point mutations in established resistance drivers *Braf*, *Nras*, *Cot*, *Pdgfrb*, *Raf1*, *Cdkn2a*, *Nf1*, *Igf1r*, *Mek1*, *Mek2* (*Map2k2*), *Pten*, or *Met* (European Nucleotide Archive accession no. ERP002600).

Genomic DNA from PLX4720-naïve and -resistant melanoma samples were subjected to splinkerette PCR and 454 sequencing to isolate common insertion sites (CISs), which were defined using Gaussian kernel convolution statistics (GKC) (30). The list of candidate drivers identified in BCTSB13 melanomas (PLX4720-naïve) (Dataset S1) included 56 statistically significant loci ($P < 0.05$; *Materials and Methods*) and many well-established melanoma driver genes including *Cdkn2a* and *Pten* (20, 21, 31–33), as well as candidate drivers such as *Atrx* and *Sox6,* which have not previously been described in melanoma. The patterns of *T2/Onc* transposon insertions in *Cdkn2a* and *Pten* (Fig. S4 *A* and *B*) were in keeping with the known biological roles for these genes in melanoma development. Furthermore, CISs also identified competitive endogenous RNAs of *Pten* such as *Zeb2* (34). Importantly, hierarchical clustering revealed that tumors collected from the same mouse were genetically independent (Fig. S4*C*).

The analysis of insertion sites from the 53 PLX4720-resistant melanomas identified 10 CISs ($P < 0.05$) (Fig. 2 and Dataset S1). We performed a Fisher's exact statistical test to compare the CIS insertions found in the PLX4720-naïve and PLX4720-resistant tumors in an attempt to identify significantly enriched loci following BRAF inhibitor treatment. This analysis yielded a list of eight CISs with a $P < 0.05$ (Fig. 2). Importantly, this list included *Braf*, *Mitf*, and *Cdkn2a*, all of which have previously been described as mediators of resistance to BRAF inhibitors in melanoma patients, thus validating the human relevance of our screen (6, 7, 35–38). In the case of the *Mitf* locus, 14 out of 15 transposon insertions (6 of which fell into the CIS, Fig. 2) were orientated such that the murine stem cell virus (MSCV) promoter will drive transcriptional up-regulation of the gene (Fig. S4*D*). The remaining candidate genes on the list have not previously been implicated in resistance to BRAF inhibitor therapy. We note that by using Fisher's exact statistics a stringent list of candidate drug resistance mediators was identified. Further candidates maybe revealed from our data using alternative approaches.

Insertional Activation of Truncated Braf Confers Resistance to PLX4720. As shown in Fig. 2, statistical analysis of PLX4720-naïve and -resistant tumors revealed a significant enrichment of transposon insertions at the *Braf* locus in resistant melanomas ($P = 3.43 \times 10^{-08}$). All nine insertions within the gene body of *Braf* in resistant tumors were oriented such that the MSCV promoter in the transposon will promote transcriptional activation of *Braf*, with most producing a truncated isoform that includes the kinase domain of *Braf* but lacks the N-terminal regulatory domain (Fig. S5*A*). Interestingly, five out of nine insertions were located in intron 9, a hotspot for transposon insertions in a previously described *Braf*-driven sarcoma model (26). We verified the existence of *Braf-T2/Onc* chimeric transcripts using primers in exon 10 ($n = 4$), 2 ($n = 2$), or 3 ($n = 1$) of *Braf* and in the splice donor of the transposon (Fig. S5*B*). We next determined whether transposons were located in the wild-type or V618E mutant allele of *Braf*. We analyzed three tumors and found two insertions in the wild-type allele and one in the mutant $Braf^{V618E}$ allele (Fig. S5*C*), suggesting that overexpression of both the wild-type and mutant kinase domain of Braf is able to confer resistance to PLX4720. Notably, intron 9 insertions generate a truncated transcript similar to an alternative splice form of *BRAF* that confers vemurafenib resistance in human melanoma patients (Fig. S5*D*) (6), further highlighting the clinical relevance of our screen.

The Proto-Oncogene *ERas* Mediates Melanoma Resistance to PLX4720 Through Activation of the AKT/BAD Pathway. The proto-oncogene *ERas* (ES cell-expressed Ras) was also discovered as a candidate drug resistance gene, with *ERas* insertions being exclusively found in PLX4720-resistant tumors and not in PLX4720-naïve controls (Fig. 2). *ERas* is a small gene spanning ∼4 kb on the X chromosome. All four transposon insertions were located in the first intron (Fig. 3*A*) and resulted in the generation of chimeric *ERas*-transposon transcripts (Fig. S6 *A* and *B*).

To validate the role of *ERAS* in resistance to PLX4720 we ectopically expressed human *ERAS* in the $BRAF^{V600E}$-mutant melanoma cell lines 451Lu and A375 by retroviral transduction and assessed survival in response to PLX4720 concentrations ranging from 0 to 100 μM. *ERAS* expression reduced sensitivity to PLX4720 in both cell lines (Fig. 3*B* and Fig. S6*C*); indeed, the concentration required to inhibit cell proliferation by 50% (GI_{50})

Gene	Chr	CIS Peak Location	CIS Height	Insertions	P-value	CIS in primaries?	Fisher's exact test
Cdkn2a	4	88924053	8.8928	9	0	Yes	0.00049
Braf	6	39598333	7.1214	11	0		3.43E-08
Mitf	6	97939190	5.6086	6	0	Yes	0.00013
Stag2	X	39593723	5.5315	8	0	Yes	0.00130
ERas	X	7504777	3.9892	4	4.9E-12		0.00652
Arhgef2	3	88417919	3.7004	4	0.0004		0.70251
Ppp6c	2	39057856	4.7912	6	0.0242		0.00043
Tsc22d2	3	58234324	4.6435	5	0.0315		0.00313
Bach2	4	32366943	4.2831	5	0.0366		0.10269
Lcor	19	41606067	4.5054	8	0.0438		0.00383

Fig. 2. Candidate resistance genes identified in the BCTSB13 resistant melanomas as CISs. Each gene is annotated by its gene symbol and chromosome of origin, along with the height of the associated CIS peak with its location and the number of insertions contributing to the CIS. *P* values are corrected for multiple testing using the count of all CIS peaks across the genome. The seventh column reports whether a gene was also associated with a CIS in the primary BCTSB13 melanomas. A Fisher's exact test was performed to assess the significance of insertion site clusters in primary vs. resistant samples. CISs are sorted by CIS height.

was 4.90 vs. 1.31 μM in 451Lu cells and 0.58 vs. 0.20 μM in A375 cells for *ERAS*-transduced cells vs. controls, respectively.

Previous work has shown that *ERas* activates the PI3K pathway, but not the MAPK pathway, when expressed in mouse ES cells or human cell lines (39, 40). Thus, we examined AKT, ERK, and MEK phosphorylation in 451Lu cells overexpressing *ERAS* and found robust AKT phosphorylation, whereas MAPK activity was unaffected (Fig. 3*C*).

Given this result, we then assessed the effect of PLX4720 or the allosteric AKT inhibitor MK2206 on the PI3K and MAPK pathways, either alone or in combination, in *ERAS*-expressing 451Lu melanoma cells and isogenic controls. As shown in Fig. 3*C*, PLX4720 treatment efficiently decreased ERK and MEK phosphorylation regardless of *ERAS* expression, whereas AKT phosphorylation was mostly unaffected. In contrast, ERAS-mediated phosphorylation of AKT was efficiently blunted by MK2206 treatment, and dual PLX4720/MK2206 treatment inhibited both the MAPK and PI3K signaling pathways (Fig. 3*C* and Fig. S7). Accordingly, dual PLX4720/MK2206 treatment negated *ERAS*-mediated resistance of 451Lu cells to PLX4720 (Fig. 3*B*). Importantly, phospho-S6, which has been shown to be a bona fide predictor of sensitivity to BRAF inhibitors (41), is reduced in control cells treated with PLX4720, rescued by *ERAS* expression, and then decreased to some extent by the combination treatment (Fig. 3*C* and Fig. S7). Notably, even though the PI3K pathway is considered to be the main regulator of S6 phosphorylation through TORC1 signaling, our data support the role of MAPK signaling in S6 phosphorylation in $BRAF^{V600E}$ melanoma cells, as recently reported (41).

Having established that *ERAS* functions through the PI3K/AKT pathway in melanoma cells we reasoned that it might confer resistance to PLX4720 by activating AKT-dependent survival signals. Therefore, we assessed the effect of PLX4720 treatment of 451Lu cells on members of the Bcl-2 family of apoptotic proteins, which have been established as important mediators of melanoma cell survival (42, 43) (Fig. 3*D*). Importantly, previous work has suggested that subtle changes in MCL1 levels play a central role in resistance to PLX4720 treatment in cells with amplified IGF1R, highlighting the key role that Bcl-2 family proteins and their downstream pathways play in resistance (12). Whereas the levels of the antiapoptotic protein MCL1 were consistently decreased following PLX4720 treatment, the levels of the proapoptotic protein BIM were increased. Interestingly, *ERAS* overexpression did not alter the expression levels of MCL1 or BIM in response to PLX4720, suggesting that these proteins do not play a dominant role in *ERAS*-mediated resistance. BAD is a proapoptotic protein whose phosphorylation at S112 and S136 results in its inactivation. Importantly, *ERAS* expression led to BAD hyperphosphorylation at both S112 and S136, suggesting a higher survival threshold (Fig. 3*D* and Fig. S7). PLX4720 treatment of *ERAS*-expressing cells resulted in decreased BAD^{S112} phosphorylation whereas phospho-BAD^{S136} remained elevated, suggesting a blunted apoptotic response in these cells. Importantly, the phosphorylation of BAD^{S136} is mainly PI3K-dependent (44) and was decreased in response to treatment with the AKT inhibitor MK2206 (Fig. 3*D* and Fig. S7). Intriguingly, BAD^{S112} phosphorylation, thought to be largely MAPK-dependent (45–47), was higher in *ERAS*-expressing cells, suggesting cross-talk between the PI3K and MAPK pathways in the regulation of this site. Nonetheless, phosphorylation of BAD^{S112} in *ERAS*-expressing cells was suppressed by PLX4720 treatment, suggesting that BAD^{S136} phosphorylation alone may be sufficient to mediate resistance to PLX4720. Only with concomitant inhibition of MAPK and AKT by combinatorial treatment with PLX4720 and MK2206 did we observe evidence of dephosphorylation of the BAD protein at both sites (Fig. 3*D* and Fig. S7). Accordingly, *ERAS* expression increased the survival of PLX4720-treated cells, a phenotype that was negated by combined treatment with PLX4720 and MK2206 (Fig. 3*E*). Thus, increased resistance of *ERAS*-expressing cells to PLX4720 is mediated, at least in part, through up-regulation of the PI3K/AKT pathway and phosphorylation/inactivation of the proapoptotic protein BAD.

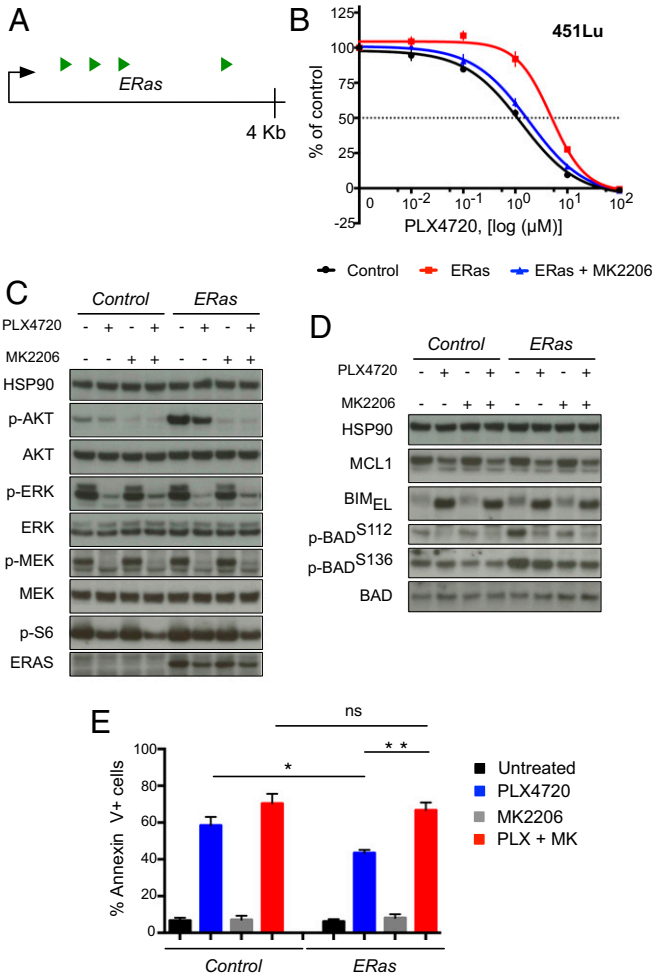

Fig. 3. *ERAS* expression confers resistance to PLX4720. (*A*) *ERas* is among the top CISs identified in melanomas from mice treated with the BRAF inhibitor PLX4720. The structure of the mouse gene (vertical bar, exon) and the position of transposon insertions are shown. The black arrow indicates the direction of *ERas* transcription. Green arrowheads indicate the orientation of transposon insertion events. The pattern of insertions is consistent with gene activation. (*B*) Drug sensitivity was measured for 451Lu ($BRAF^{V600E}$) human melanoma cells infected with an empty (control, black line) or with a human *ERAS* (red line) expression retroviral vector. A multipoint PLX4720 drug concentration scale (ranging from 0 to 100 μM) was used. Blue line indicates concomitant treatment with the AKT inhibitor MK2206 (3 μM) for *ERAS* cells. Error bars represent SEM between replicates ($n = 6$). (*C*) Western blot analysis showing that *ERas* induces phosphorylation of AKT, which can be reversed by treatment with the AKT inhibitor MK2206. Control and *ERAS*-expressing 451Lu cells were assayed after 18 h of treatment with DMSO (untreated control) or 1 μM PLX4720 or 3 μM MK2206 or the combination of them. HSP90 protein levels were used as loading control. (*D*) BAD hyperphosphorylation induced by *ERAS* expression in 451Lu cells is resolved by concomitant treatment with PLX4720 and MK2206. The experiment was performed as in *B*. (*E*) Combinatorial BRAF and AKT inhibition enhances apoptotic response in *ERAS* expressing cells. Control and *ERAS* 451Lu cells were treated with PLX4720 (3 μM), MK2206 (4 μM), or a combination of them (PLX + MK) for 72 h. Cells were then stained with Annexin-V and analyzed by flow cytometry. Mean and SEM of three independent experiments are shown. Significance was assessed using the Student's two-tailed *t* test. $*P < 0.05$; $**P < 0.01$; ns, not significant.

ABT-263 is a BAD-like BH3 mimetic compound that like BAD binds with high affinity to Bcl-xL, Bcl-2, and Bcl-w (48). In accordance with the above data, we found a statistically significant association between the basal expression of *ERAS* and the level of sensitivity to ABT-263 in the panel of 1,000 human cancer cell lines analyzed by the Genomics of Drug Sensitivity in Cancer (49) project (*Materials and Methods*). When considering subgroups of cell lines falling within extreme quantiles of *ERAS* basal expression (5% and 10%) we observed a statistically significant difference in response to ABT-263, in terms of variation of half-maximal inhibitory concentration ($P = 0.009$ and 0.0008; Fig. S8). In both cases, cell lines with high expression levels of *ERAS* were significantly more sensitive to ABT-263 compared with low *ERAS*-expressing cells (Fig. S8 and Dataset S1). We also performed the same analysis for the pan-AKT inhibitor MK2206 but no significant association was observed.

The AKT/BAD Pathway Contributes to HGF-Mediated BRAF Inhibitor Resistance. A correlation between stromal production of HGF in patients with BRAF mutant melanoma and resistance to BRAF inhibitors was recently reported. This is due to concomitant reactivation of both MAPK and PI3K pathways in melanoma cells expressing the HGF receptor MET (13, 14). Because HGF is known to regulate cell survival through PI3K-mediated phosphorylation/inhibition of BAD (50, 51), we asked whether HGF causes resistance to vemurafenib through the regulation of BAD. Therefore, we took three of the MET-expressing melanoma cell lines previously used in Straussman et al. (14) (G-361, SK-MEL-5, and SK-MEL-28) and determined the levels of BAD phosphorylation at S112 and S136 in response to PLX4720 with the addition of HGF under conditions previously shown to elicit resistance, and without HGF as a control. As previously reported, HGF treatment activated the MET receptor and reactivated both MAPK and PI3K pathways. BAD remained hyperphosphorylated following PLX4720 treatment in the context of HGF, compared with cells treated with the BRAF inhibitor alone (Fig. 4*A* and Fig. S7). The extent of the induction of BAD phosphorylation by HGF in PLX4720-treated cells seems to correlate with the level of phospho-S6, which is high in G-361 and SK-MEL-5 cells but lower in SK-MEL-28 cells. Also, because expression levels of the MET receptor were generally lower in SK-MEL-28 cells (Fig. 4*A*), this result is in accordance with the previous observation that the extent of HGF-induced drug resistance directly correlates with MET expression (13).

As a further proof of the key role of the Bcl-2 family in HGF-induced resistance to PLX4720 we asked whether resistance could be reverted by concomitant treatment with the BAD-like BH3 mimetic compound ABT-737. We measured growth of G-361, SK-MEL-5, and SK-MEL-28 cells untreated or treated with PLX4720, HGF, ABT-737, or with combinations of these compounds (Fig. 4*B*) and reveal that cells treated with HGF, PLX4720, and ABT-737 are growth-inhibited compared with HGF, PLX4720-treated cells. Thus, BAD inhibition may contribute to HGF-mediated PLX4720 resistance in melanoma.

Discussion

Here we deployed the *Sleeping Beauty* transposon system in a mouse model of melanoma to identify genes that accelerate oncogenic *Braf*-induced melanoma development, and also mediators of resistance to the BRAF inhibitor PLX4720. We identified 56 candidate loci that may promote melanoma formation in $Braf^{V618E}$ mice, including known tumor suppressors such as *Cdkn2a* and *Pten*. Moreover, we found eight candidate loci conferring resistance to PLX4720 treatment. Interestingly, both lists contained *Mitf*, which is a well-known melanoma oncogene amplified in ∼10% of primary and ∼20% of metastatic melanomas (35, 52, 53) and has been described as a mediator of drug resistance in melanoma (35–37, 54, 55).

We focused our attention on two of the candidate resistance genes identified in our in vivo screen: *Braf* and *ERas*. The identification of *Braf* in PLX4720-resistant, but not in PLX4720-naïve, tumors underscores the clinical relevance of our screen, because expression of alternative *BRAF* isoforms is associated with vemurafenib resistance in human melanoma patients (6). Interestingly, transposon insertion into the murine *Braf* gene generated truncated *Braf* transcripts (Fig. S5) that functionally resembled the alternative isoforms found in BRAF inhibitor-resistant human tumors. We observed transposon insertions in both the wild-type and $Braf^{V618E}$ alleles, suggesting that overexpression of wild-type mouse *Braf*, which is as much as 10 times less sensitive to PLX4720, is sufficient to sustain tumor growth in the presence of BRAF inhibitor treatment. In contrast, selective alteration of the oncogenic $BRAF^{V600E}$ allele is found in human melanomas with acquired BRAF inhibitor resistance.

The *ERas* (*ES cell-expressed Ras*) proto-oncogene, another gene identified from our screen, is a recently discovered member of the Ras family, which encodes a protein of 227 aa sharing 43%, 46%, and 47% identity with HRAS, NRAS, and KRAS, respectively. It was first identified as a potent oncogene in murine ES cells because of its ability to promote constitutive activation of the PI3K pathway (39). More recently, human *ERAS* has been proposed to play a role in cancers of the gastrointestinal tract (40, 56), and in vitro studies have suggested a role in the resistance of cell lines to chemotherapeutics (57, 58).

Remarkably, we identified four independent tumors with insertions in the *ERas* gene, despite its very small size (∼4 kb) ($P = 4.9 \times 10^{-12}$). We show that overexpression of *ERAS* causes hyperactivation of AKT. Importantly, the PI3K/AKT pathway is a major regulator of apoptotic cell death and cell survival. The proapoptotic protein BAD has been shown to be inactivated by AKT-mediated phosphorylation at S136 (44). Another site of BAD phosphorylation is serine 112, which is regulated by MAPK signaling (45–47), and a full apoptotic response is only achieved when both BAD^{S112} and BAD^{S136} residues are dephosphorylated through the suppression of both pathways (59). Importantly, others have proposed a role for members of the Bcl-2 family in resistance to BRAF inhibitor treatment. Villanueva et al. (12) identified MCL1 as a prosurvival factor that confers resistance to BRAF inhibition in IGF1R-overexpressing cells, whereas Paraiso et al. (15) found that intrinsic resistance to PLX4720 in *PTEN*-mutant cells was the result of suppression of BIM expression resulting in a blunted apoptotic response. Here we show that *ERAS* confers PLX4720 resistance by promoting the hyperphosphorylation of BAD^{S112} and BAD^{S136}, thus counteracting the inhibition of the MAPK pathway and dephosphorylation of BAD^{S112} alone (Figs. 3 *C* and *D* and 4*C*). Consequently, *ERAS*-expressing cells have a higher threshold for the induction of apoptosis and are less sensitive to PLX4720 treatment. Because this phenotype can be reverted using the AKT inhibitor MK2206 (Fig. 3 *D* and *E*) our data suggest a combinatorial approach to therapy in BRAF inhibitor-resistant melanomas that harbor hyperactivation of AKT. At this time a link between *ERAS* expression, BAD phosphorylation, and resistance to BRAF inhibitors is yet to be examined in patients and will require the comparison of expression/phosphoproteome data from large panels of melanomas sensitive and resistant to therapy once such data become available.

Therefore, to determine the relevance of our findings in humans, we sought to investigate the mechanism by which HGF signaling induces resistance to BRAF inhibition, because HGF is a known regulator of BAD (50, 51). Similar to our observations in the mouse, we determined that activation of HGF signaling inactivates BAD by preventing its full dephosphorylation in human melanoma cell lines. Furthermore, we determined that treatment of cells with the BAD-like BH3 mimetic compound ABT-737 partially rescues the resistance phenotype-induced by HGF, supporting the role of

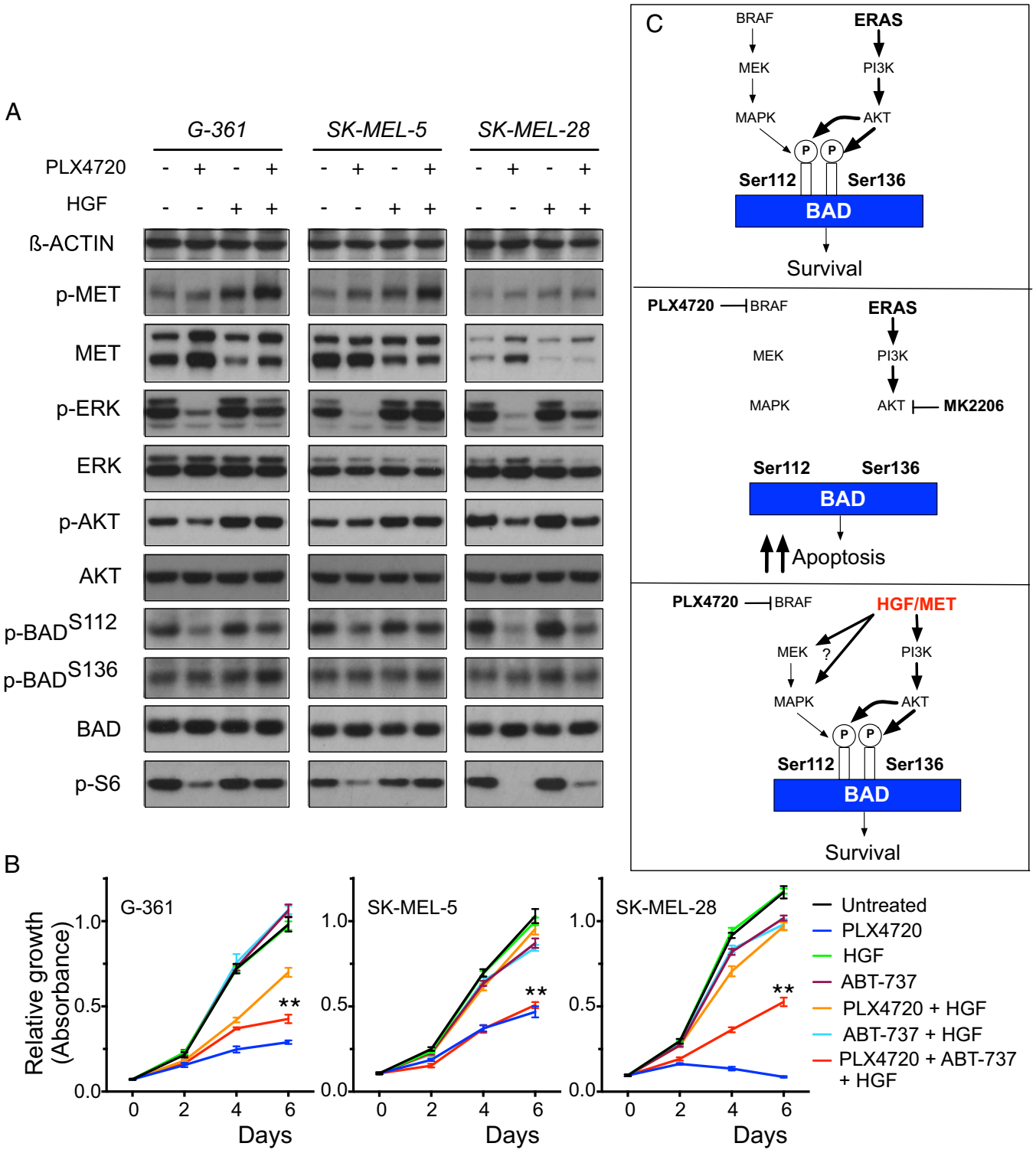

Fig. 4. HGF signaling confers resistance to PLX4720 associated with inactivation of BAD and sensitivity to ABT-737/PLX4720 combination. (*A*) Western blot analysis of the impact of HGF treatment ± PLX4720 on the phosphorylation levels of MET, ERK, AKT, BAD, and S6. G-361, SK-MEL-5, and SK-MEL-28 melanoma cell lines (*BRAF*^{V600E} mutant) were assayed after 24 h of treatment with 2 μM PLX4720 or 100 ng/mL HGF or the combination of both. β-ACTIN protein levels were used as loading control. (*B*) Growth curves of G-361, SK-MEL-5, and SK-MEL-28 cells untreated or treated with PLX4720, HGF, ABT-737, or combinations of them. Cells were seeded on day 0 and treated with drugs at day 1 and cellular proliferation was assessed by MTS assay at days 0, 2, 4, and 6. ABT-737 was used at the IC_{20} concentration as determined for each specific cell line. Compound concentrations used for G-361: 2 μM PLX-4720, 100 ng/mL HGF, and 3 μM ABT-737; for SK-MEL-5: 4 μM PLX-4720, 100 ng/mL HGF, and 2 μM ABT-737; for SK-MEL-28: 1 μM PLX-4720, 100 ng/mL HGF, and 5 μM ABT-737. Mean and SD of replicates ($n = 6$) is shown. Asterisks indicate the result of the Student two-tailed *t* test comparing cells treated with PLX4720 + HGF and cells treated with PLX4720 + HGF + ABT-737 at day 6 (**$P < 0.01$). (*C*) Schematic model showing regulation of BAD phosphorylation in melanoma. Hyperphosphorylation of BAD at S112 and S136 sites through activity of MAPK and ERAS/PI3K pathways determine cell survival (*Top*), whereas combined inhibition of these pathways by BRAF inhibitor PLX4720 and AKT inhibitor MK2206 causes BAD dephosphorylation and induction of apoptosis (*Middle*). HGF signaling is able to induce phosphorylation of BAD also in the presence of BRAF inhibition favoring cell survival and drug resistance (*Bottom*).

BAD and the Bcl-2 family in this mechanism of resistance. Because HGF-dependent resistance has been shown to operate in patients where stromal expression of HGF can be detected, our experiments suggest that regulation of the activity of BAD is relevant in determining the response of melanomas to BRAF inhibition. It should be noted that because several components of the Bcl-2 family of proteins have been linked to the response of cells to ABT-263/ABT-737, in particular MCL-1, BAX, and BIM (60, 61), a complex interplay between these proteins and BAD could mediate the overall resistance phenotype in response to HGF.

Our work represents the first example, to our knowledge, of the use of transposon-mediated mutagenesis to find mechanisms of cancer drug resistance. As illustrated here this approach has the potential to identify novel genes and mechanisms and may be particularly useful for revealing mediators of resistance to immune therapies and biotherapeutics in in vivo model systems.

Materials and Methods

Generation of the *LSL-Braf^{V618E}* Allele. See *SI Materials and Methods*.

Mice. The following alleles were used to generate the BC mouse model of melanoma: *LSL-Braf^{V618E}* (*Braf^{tm1Tuv}*), *Tyr-CreER^{T2}* [*Tg(Tyr-cre/ERT2)*13Bos] (22). BC mice were intercrossed with the following strain to generate the BCTSB13 mouse: *T2/Onc (TgTn(sb-T2/Onc)68Dla)* (26), *Rosa26-LSL-SB13* (*Gt (ROSA)26Sor$^{tm1(sb13)Tuv}$*) (28). Melanocyte-specific Cre-mediated activation of the *Braf ^{V618E}* mutant and of the SB13 transposase was obtained by topical administration of a 25 mg/mL solution of 4-OHT (70% Z-isomer; Sigma) in DMSO. The solution was applied with a paintbrush on the trunk, flanks, ears, and tail of 3-wk-old mice for two consecutive days. Size of arising melanomas was determined twice a week by caliper measurements of tumor length and width and volume was calculated using the following formula:

$$Volume = (\pi/6)(abb),$$

where *b* is the shorter of the two measurements.

Tumor weight was estimated by assuming that 1 cm^3 = 1 g.

In accordance with U.K. Home Office Regulations mice were killed when the estimated external tumor weight was maximum 10% of the body weight.

To prepare plasma samples for PK analysis of PLX4720, the mice were anesthetized with isoflurane and terminal blood samples were collected by cardiac puncture immediately before culling in tubes containing lithium heparin. After centrifugation of the blood samples plasma was then separated and frozen before the analysis. Mice were housed at a 12-h light/12-h dark cycle. All work was performed in accordance with Cancer Research UK and Wellcome Trust Sanger Institutes' Animal Welfare and Ethical Review Body (AWERB). All procedures were approved by the Home Office (UK).

CIS Analysis. Splinkerette PCRs were performed from 278 naïve and 53 PLX4720-resistant BCTSB13 melanomas as described previously (62, 63). Reads from sequenced tumors were mapped to the mouse genome assembly NCBI m37 and merged together to identify SB insertion sites. Redundant sequences, as well as insertions in the *T2/Onc* donor concatamer resident chromosome (chromosome 1), were removed. Analysis of CISs was performed as previously described (62). For the statistical analysis, non-redundant insertion sites (40,395 from naïve and 11,070 from PLX-resistant tumors) were used to identify CISs using a GKC framework (30).

Multiple kernel scales were used in the GKC framework (widths of 15,000, 30,000, 50,000, 75,000, 125,000, and 250,000 nucleotides). CISs predicted across multiple scales and overlapping in their genomic locations were clustered together, such that the CIS with the smallest genomic "footprint" was reported as the representative CIS. For highly significant CISs with narrow spatial distributions of insertion sites the 15,000 kernel is typically the scale on which CISs are identified.

Comparison of Primary and Resistant CISs. A gene-centric approach was used to assess the significance of insertion-site clusters in primary vs. resistant samples. The genomic spans of CISs were retrieved for both the primary and resistant samples. Overlapping CISs were merged into a single genomic span. Each span was then checked for the presence of a translatable gene, or genes, within the region using version 67 of the EnsEMBL mouse genome annotation database. For each overlapping gene the start and end coordinates of every potential transcript were determined.

Using the coordinates of the transcripts, counts were made of the insertion sites contained within these regions from the primary and resistant samples. Insertions were counted on the sample level (i.e., a sample could have multiple insertions within the span of transcript but the sample was only counted once). For each transcript the following single-tailed Fisher exact test was performed: number of resistant samples in transcript per number of primary samples in transcript and number of resistant samples not in transcript per number of primary samples not in transcript.

Whole-Exome Sequencing of Mouse Tumors Resistant to PLX4720. Whole-exome sequencing was performed using the Agilent SureSelect Mouse All Exon kit. Captured material was indexed and sequenced on the Illumina GAII and HiSeq2000 platforms at the Wellcome Trust Sanger Institute. Successfully sequenced reads were then aligned to the mouse reference genome (GRCm38) before base quality score recalibration and realignment around InDels. We used the Cake somatic variants detection pipeline as described previously (64). Variant calls were filtered for quality and depth and known germ-line variants were removed (65).

Detection of *ERas-T2/Onc* and *Braf-T2/Onc* Fusion mRNA by RT-PCR in SB Tumors. Mouse tissue samples were immediately placed in RNAlater solution (Qiagen) and stored for at least 24 h at 4 °C and then snap-frozen until they were processed. Total RNA was then isolated from frozen SB tumors by use of the Qiagen TissueLyser and Qiagen RNeasy Mini kit according to manufacturer instructions, and contaminating DNA was removed by treatment with RNase-Free DNase Set (Qiagen). One microgram of RNA was reverse-transcribed into cDNA using the High Capacity RNA-to-cDNA kit (Applied Biosystems). RT-PCR was carried out with a nested PCR approach using primers in the coding sequence of the mouse *ERas* or *Braf* genes and the *Foxf2* splice donor sequence of the *T2/Onc* transposon cassette. cDNA was used as a template in the first round of PCR, and the product was then used for the second round of nested PCR. PCR products were cloned into pCR-Blunt II-TOPO vector (Life Technologies) and positives clones were sequenced. PCR primer sequences are available upon request.

PLX4720 PK Bioanalysis. Plasma and tissue concentrations of drugs were determined at Integrated Analytical Solutions by extracting the sample homogenates with acetonitrile (containing internal standards), diluting with 5× volume of 0.2% formic acid, and analyzing by liquid chromatography-tandem mass spectrometry.

PLX4720 Drug Chow Preparation. PLX4720 was provided by Plexxikon and was prepared as a drug chow at Research Diets Inc. For preparation of each kilogram of rodent chow, 417 mg of PLX4720 was comixed with ingredients for the control AIN-76A purified rodent diet. PLX4720 and control chows were irradiated after preparation to control growth of microorganisms. With typical consumption the expected drug dose delivered is ~75 $mg \cdot kg^{-1} \cdot d^{-1}$.

Cell Culture. *BRAF^{V600E}* mutant human melanoma cell lines were STR-validated and mycoplasma-tested. The 451Lu and A375 cells were cultured in DMEM supplemented with 10% FCS, whereas G-361, SK-MEL-5, and SK-MEL-28 cells were cultured in RPMI supplemented with 10% FCS. BRAF inhibitor PLX4720 (Plexxikon), the AKT inhibitor MK2206, and the BAD-like BH3 mimetic compound ABT-737 (Selleckchem) were dissolved in DMSO and used as indicated. HGF (Sigma) was dissolved in PBS containing 0.2% BSA, sterile-filtered, and used at 100 ng/mL.

To generate mouse embryo fibroblasts (MEFs) E13.5-E14.5 embryos were eviscerated, minced in 0.25% trypsin, and passed through pipettes to generate single-cell suspensions. MEFs were cultured in DMEM supplemented with 10% (vol/vol) FCS. MEFs were infected with adenoviruses containing Cre or Flpe recombinases or empty control purchased from the University of Iowa Gene Transfer Vector Core facility.

Cell Viability and Apoptosis Assays. For cell viability assay cells were seeded into 96-well plates (1,000 cells per well for 451Lu line or 500 cells per well for A375 line). Twenty-four hours later cells were treated with increasing concentration of PLX4720 (0.01–100 μM) with or without the presence of 3 μM MK2206 and incubated for 4 d. Six replicates were performed for each cell line and drug combination. At the end of the incubation cell viability was measured using the CellTiter 96 Aqueous One Solution Cell Proliferation Assay (Promega) according to manufacturer instructions. Absorbance readings were subtracted from the value of blank wells and the reduction in cell growth was calculated as a percentage of absorbance in the absence of any

drug. Data were analyzed using a nonlinear regression curve fit with a sigmoidal dose response using GraphPad Prism 6 software.

For apoptosis analysis melanoma cells were treated with 3 μM PLX4720 and/or 4 μM MK2206 for 72 h. Cells were then detached with Accutase (Millipore) and stained with Annexin V Alexa Fluor 488 Conjugate and SYTOX AADvanced Dead Cell Stain Kit (Life Technologies) according to manufacturer instructions. Samples were subsequently analyzed with an LSRFortessa (BD) apparatus.

Correlation Between *ERAS* Basal Expression and Drug Response in Human Cancer Cell Lines. To evaluate the extent of correlation between the basal expression of *ERAS* and response to drug treatment in human cancer cell lines we made use of a large-scale drug screening dataset from the Genomics of Drug Sensitivity in Cancer project (49). In this study a large collection of ∼1,000 genomically characterized human cancer cell lines has been screened for reduction in viability after 72 h of treatment with ∼140 different compounds at nine different concentrations. From this dataset we extracted IC_{50} (i.e., half-maximal inhibitory concentration) values. Additionally, we obtained the basal expression profiles for the panel of cell lines in the same study. From the raw CEL files we computed normalized gene expression intensities by using the robust multiarray average method (66).

Finally, we further normalized the resulting expression datasets genewisely as follows. We first estimated the probability distribution P_g describing the expression of a given gene g across the cell lines by using a nonparametric Gaussian kernel estimator. Then we assigned to each expression values $x_{g,l}$ (of gene g in cell line l) a normalized expression score equal to

$$z_{g,l} = log\left(\frac{CDF_g(x_{g,l})}{1 - CDF_g(x_{g,l})}\right),$$

where $CDF_g(x)$ is the cumulative distribution of gene g at x.

Finally, for the drug association test, we considered two groups of cell lines, the first corresponding to samples falling within the n^{th} percentile of *ERAS* normalized expression and the second corresponding to samples falling over the $(100 - n)^{th}$ percentile of *ERAS* normalized expression (for $n = 5$ and 10). Then we performed an unpaired Welch's t test considering as dependent variable the IC_{50} value of the drug under consideration across the cell lines in the two defined quantiles and the resulting groups as factors.

Senescence-Associated β-Gal Staining. *LSL-Braf*^{V618E} MEFs were fixed in 2% formaldehyde/0.2% glutaraldehyde in PBS for 5 min and stained in staining solution (citric acid/phosphate buffer pH 6.0, 150 mM NaCl, 2 mM MgCl, 5 mM potassium ferricyanide, 5 mM potassium ferrocyanide, and 1 mg·mL^{-1} X-gal) overnight at 37 °C. Fields of at least 50 cells were counted, in triplicate.

Plasmids and Retroviral Infections. The human *ERAS* full-length cDNA was purchased as a TrueORF (OriGene) and sequence-verified. It was then subcloned into a *pBabe* Puro retroviral vector. To prepare retrovirus, packaging Phoenix cells were seeded and transfected 24 h later using the ProFection Mammalian Transfection System Calcium Phosphate kit (Promega). Human melanoma target cells were infected with retroviruses produced in the packaging cells (24 and 48 h after transfection) in the presence of 8 μg/mL Polybrene (Millipore) and were selected with 1 μg/mL Puromycin (Life Technologies).

Western Blotting. Cells were washed three times in cold PBS and protein lysates were obtained by the use of RIPA buffer with protease and phosphatase inhibitors (Cell Signaling). Equivalent amounts of protein were resolved in 4–12% gradient SDS/PAGE gels (Life Technologies), transferred to Immobilon-P Transfer Membranes (Millipore), and incubated with the following primary antibodies: HSP90 (4875, lot number 3), phospho-ERK1/2$^{T202/Y204}$ (4370, lot number 12), ERK1/2 (4695, lot number 8), phospho-AKT^{S473} (4060, lot number 16), AKT (9272, lot number 24), phospho-MEK1/2^{S221} (2338, lot number 6), MEK1/2 (9122, lot number 7), phospho-S6$^{S235/S236}$ (2211, lot number 5), MCL1 (4572, lot number 4), BIM (2819, lot number 6), phospho-BAD^{S112} (5284, lot number 3), phospho-BAD^{S136} (5286, lot number 4), phospho-MET$^{Tyr1234/1235}$ (3077, lot number 6), and MET (8198, lot number 4) from Cell Signaling; Actin (sc-1615, lot number I1508) and BAD (sc-7869, lot number H1810) from Santa Cruz Biotechnology; and ERAS (AP1470a, lot number SHO71102T) from Abgent. Membranes were then incubated with secondary horseradish peroxidase antibodies (Jackson ImmunoResearch) and developed by use of the ECL detection system (GE Healthcare). Western blot signals have been quantified by scanning densitometry with ImageJ software.

PCR and Southern Blot. PCR and Southern blot analyses were carried out in accordance with standard techniques.

Histology and Immunohistochemistry. Tissues were fixed in 10% neutral buffered formalin for 24 h and transferred to 70% ethanol. Tissues were embedded in paraffin, and 3- to 5-μm sections were processed for hematoxylin–eosin staining and immunohistochemistry.

Antigen retrieval was heat-mediated using citrate buffer at pH 6.0. Endogenous peroxidases were blocked with 3% hydrogen peroxide, followed by serum and avidin–biotin blocking. Primary antibodies were incubated overnight at 4 °C. Secondary antibodies were incubated at room temperature for 30 min. Antigens were developed with Vectastain ABC reagents and peroxidase substrate DAB kit (Vector Labs). Primary antibodies used were anti-S100 (1:1,000; Dako) and MITF (1:50; Santa Cruz). Slides were counterstained with hematoxylin.

ACKNOWLEDGMENTS. We thank Amary Wagner for help in early characterization of the model, Jos Jonkers and Sjors Kas for help with the splinkerette PCRs, and Jelle ten Hoeve for bioinformatics support. D.P., F.A.K., A.G.R., P.A. P.-M., M.J.A., D.A.T., and D.J.A. were supported by Cancer Research UK. D.J.A. was also supported by the Wellcome Trust, D.P. by an Intra-European Marie Curie Fellowship and an International Fellowship in Cancer Research from the Italian Association for Cancer Research, and F.A.K. by a Boehringer Ingelheim Fonds PhD fellowship. This work is supported by the European Research Council Synergy Programme.

1. Davies H, et al. (2002) Mutations of the BRAF gene in human cancer. *Nature* 417(6892):949–954.
2. Bollag G, et al. (2010) Clinical efficacy of a RAF inhibitor needs broad target blockade in BRAF-mutant melanoma. *Nature* 467(7315):596–599.
3. Chapman PB, et al.; BRIM-3 Study Group (2011) Improved survival with vemurafenib in melanoma with BRAF V600E mutation. *N Engl J Med* 364(26):2507–2516.
4. Flaherty KT, et al. (2010) Inhibition of mutated, activated BRAF in metastatic melanoma. *N Engl J Med* 363(9):809–819.
5. Sosman JA, et al. (2012) Survival in BRAF V600-mutant advanced melanoma treated with vemurafenib. *N Engl J Med* 366(8):707–714.
6. Poulikakos PI, et al. (2011) RAF inhibitor resistance is mediated by dimerization of aberrantly spliced BRAF(V600E). *Nature* 480(7377):387–390.
7. Shi H, et al. (2012) Melanoma whole-exome sequencing identifies (V600E)B-RAF amplification-mediated acquired B-RAF inhibitor resistance. *Nat Commun* 3:724.
8. Nazarian R, et al. (2010) Melanomas acquire resistance to B-RAF(V600E) inhibition by RTK or N-RAS upregulation. *Nature* 468(7326):973–977.
9. Emery CM, et al. (2009) MEK1 mutations confer resistance to MEK and B-RAF inhibition. *Proc Natl Acad Sci USA* 106(48):20411–20416.
10. Whittaker SR, et al. (2013) A genome-scale RNA interference screen implicates NF1 loss in resistance to RAF inhibition. *Cancer Discov* 3(3):350–362.
11. Johannessen CM, et al. (2010) COT drives resistance to RAF inhibition through MAP kinase pathway reactivation. *Nature* 468(7326):968–972.
12. Villanueva J, et al. (2010) Acquired resistance to BRAF inhibitors mediated by a RAF kinase switch in melanoma can be overcome by cotargeting MEK and IGF-1R/PI3K. *Cancer Cell* 18(6):683–695.
13. Wilson TR, et al. (2012) Widespread potential for growth-factor-driven resistance to anticancer kinase inhibitors. *Nature* 487(7408):505–509.
14. Straussman R, et al. (2012) Tumour micro-environment elicits innate resistance to RAF inhibitors through HGF secretion. *Nature* 487(7408):500–504.
15. Paraiso KH, et al. (2011) PTEN loss confers BRAF inhibitor resistance to melanoma cells through the suppression of BIM expression. *Cancer Res* 71(7):2750–2760.
16. Haq R, et al. (2013) BCL2A1 is a lineage-specific antiapoptotic melanoma oncogene that confers resistance to BRAF inhibition. *Proc Natl Acad Sci USA* 110(11): 4321–4326.
17. Ye Y, et al. (2013) Loss of PI(4,5)P2 5-phosphatase A contributes to resistance of human melanoma cells to RAF/MEK inhibitors. *Transl Oncol* 6(4):470–481.
18. Shao Y, Aplin AE (2010) Akt3-mediated resistance to apoptosis in B-RAF-targeted melanoma cells. *Cancer Res* 70(16):6670–6681.
19. Hilmi C, et al. (2008) IGF1 promotes resistance to apoptosis in melanoma cells through an increased expression of BCL2, BCL-X(L), and survivin. *J Invest Dermatol* 128(6): 1499–1505.
20. Dankort D, et al. (2009) Braf(V600E) cooperates with Pten loss to induce metastatic melanoma. *Nat Genet* 41(5):544–552.
21. Dhomen N, et al. (2009) Oncogenic Braf induces melanocyte senescence and melanoma in mice. *Cancer Cell* 15(4):294–303.
22. Bosenberg M, et al. (2006) Characterization of melanocyte-specific inducible Cre recombinase transgenic mice. *Genesis* 44(5):262–267.
23. Wojnowski L, et al. (1997) Endothelial apoptosis in Braf-deficient mice. *Nat Genet* 16(3):293–297.
24. Pollock PM, et al. (2003) High frequency of BRAF mutations in nevi. *Nat Genet* 33(1): 19–20.

25. Patton EE, et al. (2005) BRAF mutations are sufficient to promote nevi formation and cooperate with p53 in the genesis of melanoma. *Curr Biol* 15(3):249–254.
26. Collier LS, Carlson CM, Ravimohan S, Dupuy AJ, Largaespada DA (2005) Cancer gene discovery in solid tumours using transposon-based somatic mutagenesis in the mouse. *Nature* 436(7048):272–276.
27. Dupuy AJ, Akagi K, Largaespada DA, Copeland NG, Jenkins NA (2005) Mammalian mutagenesis using a highly mobile somatic Sleeping Beauty transposon system. *Nature* 436(7048):221–226.
28. Pérez-Mancera PA, et al.; Australian Pancreatic Cancer Genome Initiative (2012) The deubiquitinase USP9X suppresses pancreatic ductal adenocarcinoma. *Nature* 486(7402):266–270.
29. Tsai J, et al. (2008) Discovery of a selective inhibitor of oncogenic B-Raf kinase with potent antimelanoma activity. *Proc Natl Acad Sci USA* 105(8):3041–3046.
30. de Ridder J, Uren A, Kool J, Reinders M, Wessels L (2006) Detecting statistically significant common insertion sites in retroviral insertional mutagenesis screens. *PLOS Comput Biol* 2(12):e166.
31. van den Hurk K, et al. (2012) Genetics and epigenetics of cutaneous malignant melanoma: A concert out of tune. *Biochim Biophys Acta* 1826(1):89–102.
32. Kamb A, et al. (1994) Analysis of the p16 gene (CDKN2) as a candidate for the chromosome 9p melanoma susceptibility locus. *Nat Genet* 8(1):23–26.
33. Tsao H, Zhang X, Benoit E, Haluska FG (1998) Identification of PTEN/MMAC1 alterations in uncultured melanomas and melanoma cell lines. *Oncogene* 16(26): 3397–3402.
34. Karreth FA, et al. (2011) In vivo identification of tumor- suppressive PTEN ceRNAs in an oncogenic BRAF-induced mouse model of melanoma. *Cell* 147(2):382–395.
35. Garraway LA, et al. (2005) Integrative genomic analyses identify MITF as a lineage survival oncogene amplified in malignant melanoma. *Nature* 436(7047):117–122.
36. Johannessen CM, et al. (2013) A melanocyte lineage program confers resistance to MAP kinase pathway inhibition. *Nature* 504(7478):138–142.
37. Smith MP, et al. (2013) Effect of SMURF2 targeting on susceptibility to MEK inhibitors in melanoma. *J Natl Cancer Inst* 105(1):33–46.
38. Shi H, et al. (2014) Acquired resistance and clonal evolution in melanoma during BRAF inhibitor therapy. *Cancer Discov* 4(1):80–93.
39. Takahashi K, Mitsui K, Yamanaka S (2003) Role of ERas in promoting tumour-like properties in mouse embryonic stem cells. *Nature* 423(6939):541–545.
40. Liu Y, et al. (2013) Role of the ERas gene in gastric cancer cells. *Oncol Rep* 30(1):50–56.
41. Corcoran RB, et al. (2013) TORC1 suppression predicts responsiveness to RAF and MEK inhibition in BRAF-mutant melanoma. *Sci Transl Med* 5(196):196ra198.
42. Boisvert-Adamo K, Aplin AE (2008) Mutant B-RAF mediates resistance to anoikis via Bad and Bim. *Oncogene* 27(23):3301–3312.
43. Boisvert-Adamo K, Longmate W, Abel EV, Aplin AE (2009) Mcl-1 is required for melanoma cell resistance to anoikis. *Mol Cancer Res* 7(4):549–556.
44. Datta SR, et al. (1997) Akt phosphorylation of BAD couples survival signals to the cell-intrinsic death machinery. *Cell* 91(2):231–241.
45. Bonni A, et al. (1999) Cell survival promoted by the Ras-MAPK signaling pathway by transcription-dependent and -independent mechanisms. *Science* 286(5443): 1358–1362.
46. Fang X, et al. (1999) Regulation of BAD phosphorylation at serine 112 by the Ras-mitogen-activated protein kinase pathway. *Oncogene* 18(48):6635–6640.
47. Scheid MP, Schubert KM, Duronio V (1999) Regulation of bad phosphorylation and association with Bcl-x(L) by the MAPK/Erk kinase. *J Biol Chem* 274(43):31108–31113.
48. Tse C, et al. (2008) ABT-263: A potent and orally bioavailable Bcl-2 family inhibitor. *Cancer Res* 68(9):3421–3428.
49. Garnett MJ, et al. (2012) Systematic identification of genomic markers of drug sensitivity in cancer cells. *Nature* 483(7391):570–575.
50. Liu Y (1999) Hepatocyte growth factor promotes renal epithelial cell survival by dual mechanisms. *Am J Physiol* 277(4 Pt 2):F624–F633.
51. Kakazu A, Chandrasekher G, Bazan HE (2004) HGF protects corneal epithelial cells from apoptosis by the PI-3K/Akt-1/Bad- but not the ERK1/2-mediated signaling pathway. *Invest Ophthalmol Vis Sci* 45(10):3485–3492.
52. Lister JA, et al. (2014) A conditional zebrafish MITF mutation reveals MITF levels are critical for melanoma promotion vs. regression in vivo. *J Invest Dermatol* 134(1): 133–140.
53. Yokoyama S, et al. (2011) A novel recurrent mutation in MITF predisposes to familial and sporadic melanoma. *Nature* 480(7375):99–103.
54. Hertzman Johansson C, et al. (2013) Association of MITF and other melanosome-related proteins with chemoresistance in melanoma tumors and cell lines. *Melanoma Res* 23(5):360–365.
55. McGill GG, et al. (2002) Bcl2 regulation by the melanocyte master regulator Mitf modulates lineage survival and melanoma cell viability. *Cell* 109(6):707–718.
56. Kubota E, et al. (2010) Role of ES cell-expressed Ras (ERas) in tumorigenicity of gastric cancer. *Am J Pathol* 177(2):955–963.
57. Aoyama M, Kataoka H, Kubota E, Tada T, Asai K (2010) Resistance to chemotherapeutic agents and promotion of transforming activity mediated by embryonic stem cell-expressed Ras (ERas) signal in neuroblastoma cells. *Int J Oncol* 37(4):1011–1016.
58. Kubota E, et al. (2011) ERas enhances resistance to CPT-11 in gastric cancer. *Anticancer Res* 31(10):3353–3360.
59. She QB, et al. (2005) The BAD protein integrates survival signaling by EGFR/MAPK and PI3K/Akt kinase pathways in PTEN-deficient tumor cells. *Cancer Cell* 8(4):287–297.
60. Cragg MS, et al. (2008) Treatment of B-RAF mutant human tumor cells with a MEK inhibitor requires Bim and is enhanced by a BH3 mimetic. *J Clin Invest* 118(11): 3651–3659.
61. Sale MJ, Cook SJ (2013) The BH3 mimetic ABT-263 synergizes with the MEK1/2 inhibitor selumetinib/AZD6244 to promote BIM-dependent tumour cell death and inhibit acquired resistance. *Biochem J* 450(2):285–294.
62. March HN, et al. (2011) Insertional mutagenesis identifies multiple networks of cooperating genes driving intestinal tumorigenesis. *Nat Genet* 43(12):1202–1209.
63. Uren AG, et al. (2009) A high-throughput splinkerette-PCR method for the isolation and sequencing of retroviral insertion sites. *Nat Protoc* 4(5):789–798.
64. Rashid M, Robles-Espinoza CD, Rust AG, Adams DJ (2013) Cake: A bioinformatics pipeline for the integrated analysis of somatic variants in cancer genomes. *Bioinformatics* 29(17):2208–2210.
65. Keane TM, et al. (2011) Mouse genomic variation and its effect on phenotypes and gene regulation. *Nature* 477(7364):289–294.
66. Irizarry RA, et al. (2003) Exploration, normalization, and summaries of high density oligonucleotide array probe level data. *Biostatistics* 4(2):249–264.